

Citation for published version:
Dowell, P, Akehurst, S & Burke, R 2017, 'A real-time capable mixing controlled combustion model for highly diluted conditions', *Energy*, vol. 133, pp. 1035-1049. https://doi.org/10.1016/j.energy.2017.05.171

DOI:

10.1016/j.energy.2017.05.171

Publication date: 2017

Document Version Peer reviewed version

Link to publication

Publisher Rights CC BY-NC-ND

University of Bath

Alternative formats

If you require this document in an alternative format, please contact: openaccess@bath.ac.uk

General rights

Copyright and moral rights for the publications made accessible in the public portal are retained by the authors and/or other copyright owners and it is a condition of accessing publications that users recognise and abide by the legal requirements associated with these rights.

If you believe that this document breaches copyright please contact us providing details, and we will remove access to the work immediately and investigate your claim.

Download date: 08. Mar. 2023

A Real-Time Capable Mixing Controlled Combustion Model for Highly Diluted

Conditions

P.G. Dowell, S. Akehurst, R.D. Burke*

Powertrain and Vehicle Research Centre (PVRC), Dept. of Mechanical Engineering, University of Bath, Bath, BA2 7AY, UK

*Corresponding Author contact. Email: R.D.Burke@bath.ac.uk, Tel: +441225383481

Abstract

A new real-time capable heat release rate model is presented that captures the high dilution effects of exhaust gas recirculation (EGR). The model is a Mixing Controlled Combustion type with enhancements to account for wall impingements, pilot injections, charge dilution caused by EGR at part load. The model was parameterised in two steps using a small set of measured data: the majority of model parameters were identified without EGR before identifying additional EGR related constants. The model performance was assessed based on key metrics: start of combustion; peak heat release and point of peak heat release and cylinder pressure. The model was evaluated over the full engine speed, load and EGR operating envelope and cylinder pressure metrics were predicted with R² values above 0.94. With EGR, the model was able to predict qualitatively and quantitively the performance whilst being parameterised by only by a small dataset. The model can be used to enable the engineering of robust new control algorithms and controller hardware for future engines using offline processes.

Keywords: Diesel Combustion, Real Time model, Exhaust Gas Recirculation, Engine Model

1. Introduction

Diesel engines are used in a significant proportion of automotive applications due to their inherent high efficiency compared to Gasoline engines However, Diesel engine suffer from higher emissions of nitrous oxides (NOx) and particulate matter due to the nature of the combustion processes. To address this problem, Diesel manufacturers are having to resort to an increasing number of active emissions

control technologies such as air management and exhaust gas recirculation (EGR), Lean NOx traps (LNT) and selective catalytic reduction (SCR) [1]. These systems all require careful design and management if the high efficiency of the Diesel engine is to be maintained. Virtual development of the complete system is a promising way of being able to design and optimise the engine system before development hardware is available. The virtual development can consist of many system models or of models working in parallel to real hardware, such as hardware-in-the-loop approach (HiL). Accurate and real-time capable mathematical models are a pre-requisite for this approach [2].

Combustion is the key process for any engine as it affects all other engine subsystems. Therefore, real-time capable combustion models are an essential tool to enable virtual development and HiL methodology. For example, the real-time model replaces real engine hardware and allows the engine controller to be trialled can be tested at very early stages of the design process, and much more intensely than could be achieved though real experiments. The model emulates each of the engine's sensors and actuators however, the method is underpinned by the accuracy of the mathematical model and the ability to parameterise the model based in a way that is predicts engine performance well in extrapolated regions.

The recirculation of exhaust gases (EGR) to control NOx emissions in Diesel engines poses specific challenges through thermal, chemical and dilution effects that need to be accounted for within the combustion model. EGR critically affects the combustion process by delaying ignition and reducing the reactivity of the cylinder charge [3]. These effects need to be captured in a model that can easily be parameterised using only small amounts of experimental data.

The aim of this paper is to create a crank angle resolved, real-time capable, Diesel combustion model that captures the effects of EGR. The empirical model parameters must be generally applicable and determined using only a small number of engine operating points such that they could be established from an early prototype build or from a higher order modelling environment [4, 5]. The model must be able to predict combustion with EGR rates of up to 40-60% (equivalent to up to 5% CO2 by volume

in the cylinder charge). This is relevant for small, high speed Diesel engines in passenger car and light duty truck applications for the foreseeable future.

2. Background

2.1. Reduced order combustion model types

As most combustion, related control strategies could be developed using cycle average quantities such as the peak heat release, maximum cylinder pressure and IMEP [6], the first reduced order models for real-time applications were Mean Value Engine Models (MVEM). This approach essentially used look-up tables for the cycle averaged values as a function of engine operating points (e.g. engine speed, fuelling quantity, injection timing, EGR rate...) [2, 7-9]. As these models run on a cycle-by-cycle basis, they can easily be made to run many times faster than real time [10-14]. More recently, thermodynamic based MVEMs have been proposed based on ideal thermodynamic cycles thus including a description of the physical processes and reducing the amount of empirical data required to obtain an accurate model [15]. Whilst these MVEMs do not simulate the full combustion process, they do allow key quantities such as peak pressure and temperature to be estimated.

As the computing power of HiL simulation machines increased, real-time crank-angle resolved models have been proposed that calculate the evolution of in-cylinder pressure during the engine cycle. This type of model provides a breakdown of the time related variations in cylinder conditions throughout the engine cycle. These models have the advantage of being able to estimate the average state of the charge and have been linked to emissions that capture specific mechanisms of formation of NOx [16-20] and soot [21].

These models typically comprise:

- A combustion model to predict the heat released from combustion.
- A cylinder model to calculate the gas properties and thermodynamic state of the charge.

The crank angle resolved models can be split into 2 categories: "single zone" models or quasi dimensional models.

The term single zone is expressed in italics as it refers to models that consider the heat released from combustion to influence a homogeneous pressure and temperature throughout the combustion chamber. The properties of this single zone may be calculated from the different compositions of fresh air, burnt gas and unburned fuel. One of the major challenges of these single zone models is in defining a set of model coefficients that are not specific to each operating point of the engine [22].

Quasi-dimensional models break down the combustion chamber into small packets and therefore provide a spatial decomposition of the combustion process [23-25]. Most are built on the work of Hiroyasu [26, 27]. They are still built on empirical equations and their superiority over simple models is not yet proven [22]. Recent publications presenting these types of models can run with a calculation time of less than 1s per engine cycle, but these are still too slow for real time applications [28]. Gao et al. [29] simplified a quasi-dimensional model [20] to increase the run time. They limited the number of zones to 2, thus increasing the calculation time by a factor of over 100 to nearly real-time. An alternative approach was presented by Bittle et al. [30] who used the multizone approach for calculating local gas compositions whilst maintaining a single zone model for the heat release to reduce the model calculation time.

2.2. Real-time Phenomenological combustion modelling

Crank-angle resolved Combustion models for real time simulation models typically treat the engine cylinder as a small number of control volumes, composed of gasses of various species representing the fresh air, unburnt fuel and burnt products. In a single zone more, the combustion chamber is represented by variable size control volume (Figure 1). The control volume exchanges mass through the fuel injector, the intake and exhaust valves and via blow-by flows seeping through the piston ring pack. Energy is exchanged with the control volume through the combustion of fuel, heat transfer to

the combustion chamber walls and through work transfer to the piston. Performing an energy balance on the control volume yields equation 1 [31].

$$dU = dQ_C - dQ_{HT} - dW + dH_{inl} - dH_{exh} - dH_{bb}$$

This work is focussed exclusively on the calculation of the combustion heat release term (dQ_c/dt) for a Diesel engine with EGR. The combustion models found in the literature typically fall into two categories:

- <u>Shape Functions</u>: the most common is the Wiebe model [32, 33] although other shape functions or Neural Networks are also used [9, 34]. These models aim to replicate previously measured behaviour. Sometimes the model parameters are loosely linked to physical parameters [35] but empirical correlations are almost always required [36, 37].
- Physics Based: these models are based fuel availability and an assumption of combustion process and the most common is the mixing controlled combustion (MCC) models. Although these models comprise of a significant number of empirical constants, the amount of experimental data required to parameterise these models is substantially less than for shape functions.

The shape functions have achieved a high accuracy in terms of mathematically replicating the combustion process: they have been shown to predict the angle of 50% burn (CA50) to within +/-1deg [38] and peak cylinder pressure to within 2-7% [37]. However, to achieve this level of accuracy, a significant amount of model training data is required [38]. Consequently, they are only useful if considerable amount of data can be used. The Wiebe combustion models published in the literature typically require different model parameters for each engine operating point [35, 38, 39] or use empirical correlations to describe how the parameters vary with operating condition [37, 40, 41].

The MCC model was originally proposed by Chmela and Orthaber [42] for large bore engines with the intention of introducing more physical based equations to reduce the amount of model training required. These models are based on the turbulent energy resulting from the injection of fuel and is a reasonable representation of the combustion process during the diffusion phase. However, Dec's phenomenological model of Diesel combustion defines two phases [43]:

- a premixed phase resulting from the detonation of fuel that accumulates before combustion
 the base MCC model is weak in this area [44]
- A stoichiometric diffusive combustion phase where combustion is controlled by the rate of mixing of fuel with the surroundings – well captured by the MCC model.

This means that mixing controlled combustion yields a good estimate of combustion at high loads, where much of the combustion is diffusive, but is much less accurate at part load conditions where significant amounts of fuel combustion are in the premixed mode [45-49]. Some empirical adaptations of the MCC models have been proposed based on fuel preparation [50-53], although these reintroduce the need for large training data sets. Chmela et al. [45, 47] proposed complementary models for capturing the premixed combustion on a semi-empirical basis. Katrasnik et al. [19, 53] splits the combustion into three phases by splitting the diffusion combustion into a rich combustion (in the centre of the spray) and a lean combustion (edges of the spray). Rezei et al. [54] augmented this mode with a spray model and included the effects of swirl and squish in the turbulent kinetic energy model. The accuracy of these models tends to be lower with CA50 errors typically +/-2°CA and IMEP +/-1bar [54].

An alternative MCC model has been proposed by Barba [50]. This model includes the evaporation of fuel, the flame propagation in the pre-mixed zone and mixing controlled combustion linked to the characteristic mixing frequency. This model has been the focus of several recent applications where a single set of parameters has been used across the engine operating map [18, 55, 56]. These models have accuracies for IMEP of +/-1bar, for CA50 +/-2°CA and for peak cylinder pressure +/-3bar [18, 55].

The MCC models have typically been able to be parameterised with fewer test points than the shape function equivalents [5, 55]. For specific area of the engine operating range they have been parameterised with a single set of coefficients [44, 45], typically using data from up to 20 engine operating points [18]. This means they are better suited for use earlier in the process as data for a small number of operating points can be obtained from higher order simulations [4] or from single cylinder research engines [55].

2.3. Accounting for EGR in combustion models

EGR presents a significant challenge for MCC combustion modelling as the dilution emphasizes premixed combustion. In displacing the fresh air, EGR will reduce the available oxygen in the cylinder (dilution effect), increase the thermal capacity of the trapped gases (thermal effect) and increase dissociations reactions (chemical effect) [57-62]. The net result of EGR on apparent heat release is illustrated in Figure 2 for a 2.0L Diesel engine operating at a low load. Ignition delay is increased meaning more fuel will contribute to premixed combustion but the peak heat release is reduced as the volume of the combustion flame is larger (dilution effect) and the gases in the flame have a high specific heat (thermal effect).

In practice, EGR also affects the engine breathing characteristics because of thermal throttling [61] and high levels of EGR also cause an increase in cycle-to-cycle and cylinder-to-cylinder variability, reducing engine stability [63].

For shape function heat release models which are calculated at each engine operating point, the effects of EGR are captured in the individual coefficient that describe any operating point with EGR [38]. For those models seeking correlations between Wiebe coefficients and operating point, the EGR rate has been used explicitly [38, 40]. Finesso and Spessa also calibrated their empirical model over six operating points, but focussed their model only on part of the engine operating envelope [51]. The combustion delay parameters for pilot and main injections were estimated as empirical functions of

charge density, oxygen concentration and fuel injection pressure. This approach has also been adapted for from phenomenological models [50, 52, 64].

Correction factors to the MCC combustion models have also been proposed to account for EGR have been proposed [46, 48] and implemented in some models. The simplest approach consists of implementing EGR adjustment factors to the diffusion combustion [46, 48, 65, 66]. Wurzenberger and Poetsch applied the MCC model with EGR corrections to a 5 cylinder, 2.5L Diesel engine [66] and tuned the model parameters over six engine operating points, however it is unclear how many test points (EGR rates, injection timings etc.) were used at each operating point.

For the phenomenological models built on the works of Barba, EGR effects are accounted for explicitly as the fraction of burnt gases influences the ignition delay and the equivalence ratio influences the diffusion combustion [50-53, 55, 56].

This study will apply a MCC model including several model correction factors to the full speed/load/EGR operating envelope of a 2.0L Diesel engine using only a small, but carefully selected, dataset for model training. A model built on the works of Chmela is chosen as it is mathematically simpler than the models based on the works of Barba [50] which is therefore more suited to the real-time requirement. The combustion model will be described; then the model parameterisation process will be detailed. Finally, the model performance will be assessed over the full engine operating range.

3. Combustion model

The combustion model is constructed as a combination of models proposed individually in the literature. Their combination is described in detail in the following section. The key novelty of this work lies in the use of a simple parameter for the incorporation of EGR that is parameterised using only a single EGR sweep at one engine operating condition, but that can extrapolate across the full EGR operating region. The model performance in extrapolation will be presented and analysed in detail in section 5.

3.1. Base Combustion model

The base heat release model considers separately the pre-mixed combustion and the diffusive combustion such that the total heat release is the sum of the two (equation 2).

$$\frac{dQ_c}{dt} = \frac{dQ_{pre}}{dt} + \frac{dQ_{diff}}{dt}$$

The control volume is assumed to be a homogeneous mixture of gases at a single temperature and pressure and having the thermodynamic properties of the weighted average of the gas composition. With knowledge of each of the terms in the right-hand side of equation 1, the change in internal energy of the control volume can be estimated, if the charge behaves as a perfect gas. The heat loss at the cylinder walls was modelled using the work of Finol [67] with cylinder temperature imposed from measurements.

The premixed combustion is calculated using the build-up of fuel during the ignition delay (equation 3 [45, 47]) which includes:

- A term describing the reaction rate of the mixture
- An exponential term capturing the heating of the fuel
- The potential thermal energy available in injected fuel
- A quadratic term that captures the time elapsed since start of combustion to describe the initial burn rate.

$$\frac{dQ_{pre}}{dt} = a_1 \frac{\lambda \cdot AFR_{stoich}}{V_{mix}} e^{-a_2 \frac{T_a}{T_{cyl}}} m_{pre,avail}^2 LCV (t - t_{SOC})^2$$

$$where \ V_{mix} = m_{pre,avail} \left(\frac{1}{\rho_{f,vap}} + \frac{\lambda \cdot AFR_{stoich}}{\rho_{cyl}} \right)$$

The mean equivalence ratio in the mixture cloud, λ , is a model parameter that is assumed to be 0.5 for pre-mixed combustion for both main and pilot combustions.

Before the start of combustion, the mass of fuel that is available for pre-mixed combustion is calculated as a proportion of the fuel injected into the cylinder, less the amount of fuel that may have already burnt (during a previous injection). After the start of combustion, it is assumed that all subsequent injected fuel burns in a diffusive mode (equation 4). The proportion of fuel dedicated to the pre-mixed combustion, x_{pre} , was determined empirically but assumed to be constant for all operating points.

$$m_{pre,avail} = \begin{cases} x_{pre} \int\limits_{SOI}^{\theta} dm_{f,inj} - \frac{Q_{pre}(t)}{LCV} & \theta < \theta_{SOC} \\ 0 & \theta \ge \theta_{SOC} \end{cases}$$

The amount of fuel contributing to the pre-mixed combustion is primarily determined by the ignition delay period. This is the period after the start of injection but before the start of combustion. During this period, the liquid fuel injected into the cylinder is mixed with surrounding cylinder charge, evaporated, and heated up to its self-ignition temperature – this is termed the physical ignition delay. Preliminary chemical reactions also occur during this period prior to ignition – this is represented by the chemical ignition delay. Ignition is determined by the contribution of both these parameters according to equation 5: start of combustion occurs when the integral term reaches unity [56].

$$\int_{SOI}^{SOC} \frac{1}{\tau_{ID}} dt = 1, \text{ where } \tau_{ID} = \tau_{ph} + \tau_{ch}$$

The two delay terms are calculated according to the Arrhinius and Magnussen delay terms given in equations 6 and 7 [45, 68, 69]. The chemical delay is linked to the ratio of temperature to activation temperature which drives the chemical reactions. The physical delay is primarily driven by turbulence

in the cylinder which promotes the heating of the fuel. Both delay terms are scaled by a measure of the concentration of fuel and oxygen.

$$\frac{1}{\tau_{ch}} = C_{arr}c_f c_0 e^{-\frac{a_3 T_a}{T_{cyl}}} \tag{6}$$

$$\frac{1}{\tau_{ph}} = C_{mag} c_f \frac{\sqrt{k}}{\sqrt[3]{V_{cyl}}}$$
 7

where
$$c_f = \frac{m_f}{V_{mix}}$$
, $c_o = \frac{0.232 m_{cyl}}{V_{mix}}$

The diffusion combustion model is equivalent to the original MCC [42] (equation 8). The rate of heat release is linked to the amount of fuel available for combustion and the rate of mixing, described through an empirical turbulent kinetic energy term. This assumes that the turbulent energy comes from the piston motion (engine speed) and the fuel injection. It also includes a factor for spray impingement onto the cylinder wall [70].

$$\frac{dQ_{diff}}{dt} = C_{wall} \cdot C_{mod} \cdot LCV \cdot m_{f,diff,avail} \left(\frac{\sqrt{k}}{\sqrt[3]{V_{cyl}}} \right)$$

The mass of fuel available for diffusive combustion is the mass of non-combusted fuel that has been injected into the cylinder and that has evaporated as described by equation 9.

$$m_{f,diff,avail} = \int_{SOI}^{\theta} dm_{f,diff,vap} - \frac{Q_{diff}}{LCV}$$

The evaporation rate of fuel is dependent on temperature, turbulent motion and droplet size and is captured through equation 10.

$$\frac{dm_{f,diff,vap}}{d\theta} = \frac{1}{6N_{eng}} \int_{SOI}^{\theta} \frac{\left(T_{cyl}\right)^{3.3} k}{C_{evap} d_{noz}} m_{f,diff,liqu}$$
 10

The turbulent energy density k is calculated from the turbulent energy caused by fuel injection and the energy dissipated within the cylinder as in [42].

The mass of liquid fuel available for evaporation is determined as the amount of fuel dedicated for diffusive combustion that has been injected into the cylinder but has not yet evaporated (equation

11).

$$m_{f,diff,liqu} = \begin{cases} (1 - x_{pre}) \int_{SOI}^{\theta} dm_{f,inj} - m_{f,diff,vap} & \theta < \theta_{SOC} \\ soc & \theta \\ (1 - x_{pre}) \int_{SOI}^{SOC} dm_{f,inj} + \int_{SOC}^{\theta} dm_{f,inj} - m_{f,diff,vap} & \theta \ge \theta_{SOC} \end{cases}$$

3.2. Extension to combustion model for EGR

3.2.1. Thermal Effect

The thermodynamic properties of the charge due to the displacement of oxygen by CO_2 and water account for the thermal effects of EGR (changes heat capacity). At any given point, the total cylinder mass is composed of a mixture of three species: fresh air, burnt gas and unburnt fuel. The thermodynamic properties of specific heats (C_p , C_V and γ) and specific internal energy (u) each were calculated as a function of cylinder temperature [59]. The average thermodynamic properties of the cylinder were calculated by equation 12. The specific gas constant in the cylinder, R_{cyl} , was also calculated in this way taking gas constants for the air, fuel and burnt gases to be 287.05J/kgK [31], 55.95J/kgK and 285.4J/kgK [71] respectively.

$$c_{p,cyl} = Y_{air}c_{p,air} + Y_fc_{p,f} + Y_bc_{p,b}$$

$$where Y_{air} + Y_f + Y_b = 1$$

The mass fraction terms, *Y*, are calculated based on the mass of the particular species and the total mass in the cylinder

$$Y_{air} = \frac{m_{air,cyl}}{m_{cyl}}, \qquad Y_f = \frac{m_{f,cyl}}{m_{cyl}}, \qquad Y_b = \frac{m_{b,cyl}}{m_{cyl}}$$

The composition of the cylinder when the intake valve closed was determined from the concentrations in the intake manifold and a filling and emptying model (see section 3.2.4). After intake valve closing, the masses of the individual components will evolve as follows:

- Fresh air mass will reduce as the air is burnt. In addition, any blow by flows or flows through the exhaust vale will also reduce the aim mass:

$$dm_{air,cyl} = -\frac{dQ_c}{LCV}(AFR_{stoich}) - Y_{air,cyl}(dm_{exh} + dm_{bb})$$
14

- Fuel mass will increase at the rate at which it is injected into the cylinder, but reduce at the rate at which it is burnt:

$$dm_{f,cyl} = dm_{f,inj} - \frac{dQ_c}{LCV}$$
 15

- Burnt gas mass will increase following the combustion of fuel and fresh air but reduce by any blow-by or exhaust valve flows:

$$dm_{b,cyl} = \frac{dQ_c}{LCV} (1 + AFR_{stoich}) - Y_{b,cyl} (dm_{exh} + dm_{bb})$$
16

At any point, the change in total mass in the cylinder is the sum of the change in air, fuel and burnt gas masses

$$dm_{cyl} = dm_{air,cyl} + dm_{f,cyl} + dm_{b,cyl}$$
 17

3.2.2. Dilution Effect

Both ignition delay, pre-mixed and diffusive combustion are affected by the mixing of injected fuel with the surrounding gases such that sufficient oxygen is available. The dilution effect of EGR reduces the availability of oxygen and therefore interferes with this process.

For ignition delay, closer inspection of the term c_o in equation 6 shows that the numerator represents the mass of oxygen in the cylinder. To account for the reduced oxygen in the cylinder, this should be augmented according to equation 18.

$$c_{o,EGR} = \frac{0.232m_{cyl}}{V_{mix}} \left(AFR_{stoich} (1 - \chi_{EGR}) \right)$$
 18

Where χ_{EGR} is the fraction of EGR by mass as defined in equation 24.

The dilution effect will also influence the pre-mixed combustion by affecting the propagation of the flame front and the diffusion combustion because more gas must be mixed into the combustion flame increasing its volume. Equations 3 and 8 are therefore modified into equations 19 and 20 respectively to account for these effects [46, 48].

$$\frac{dQ_{pre}}{dt} = a_1 \frac{\lambda \cdot AFR_{stoich}}{V_{mix}} e^{-a_2 \frac{T_a}{T_{cyl}}} m_{pre,avail}^2 LCV (t - t_{SOC})^2 (1 - \chi_{EGR})^{a_4}$$
19

$$\frac{dQ_{diff}}{dt} = C_{mod} \cdot LCV \cdot m_{f,diff,avail} \left(\frac{\sqrt{k}}{\sqrt[3]{V_{cyl}}}\right) (1 - \chi_{EGR})$$
20

3.2.3. Chemical effect

The chemical effect of EGR is considered only minor and difficult to implement in a single zone model where only average cylinder temperature is calculated as the dissociation reactions rely on peak local cylinder temperatures. Considering the real-time nature of the proposed heat release model, these parameters are ignored.

3.2.4. Modelling external flow of EGR

Although this work considers only the effects of EGR on the combustion heat release in the cylinder, the external flow of EGR is an important parameter as it affects the composition of the gas when the intake valve closes. The EGR layout for the engine in this study is shown in Figure 3. This was modelled by considering four control volumes: the cylinder, intake and exhaust manifolds, and the EGR cooler. [72]. It is important to note that the model includes experimentally validated models for:

- Exhaust manifold heat transfer was calculated by forced convection using the Nusselt/Reynolds correlation [73] and an empirical wall temperature model.
- EGR Valve flow coefficient was captured by an empirical quadratic function expressing effective valve area to valve lift.
- EGR cooler effectiveness was mapped as a function of EGR mass flow rate based on measured gas temperatures.

4. Experimental Approach

4.1. Engine installation and operating points

Experiments were conducted on a 2.0L turbocharged, common rail Diesel engine installed on a transient engine dynamometer. A summary of the engine specification is given in Table 1. After the warm up phase of 20 minutes at mid-speed, mid-load to ensure that engine coolant and oil were at stabilised temperatures, the engine was taken to each steady-state speed/torque operating point as detailed in Figure 4. At each point the engine was held for a settling period of 5 minutes before recording operating data – this was required to achieve thermal stability at the operating point in question. For tests without EGR, low frequency data was recorded for a period of 30seconds and incylinder data was measured over 100 consecutive engine cycles. Diesel combustion, especially in the absence of EGR, is very stable unlike petrol combustion which justifies the low number of cycles. When EGR is introduced, combustion stability decreases because the recirculation of exhaust gases cause interactions between subsequent combustion cycles. With high levels of EGR, the standard deviation of pressure during combustion can increase by a factor of 2.5 [66]. To account for this, the number of combustion cycles recorded was increased to 300 for the tests with EGR.

Table 1 - Specification of the 2.0L Diesel Engine

Engine Type	Turbocharged diesel
Cylinders	4
Capacity	1998сс
Stroke	86mm
Bore	86mm
Conrod Length	152mm
Firing Order	1-3-4-2
Compression Ratio	16
Max Torque	320Nm at 1800-2000rpm
Max Power	95kW at 3800rpm
Fuel Injection	Common rail direct injection up to 1600bar

For every point the engine map in Figure 4, data was captured with no external EGR flow. Figure 4 also highlights the sub-region of the engine operating map where EGR tests were conducted. For points within the EGR test region, measurements were taken at different EGR rates, varied in five equal steps between no EGR and the maximum EGR rate at that point. Whilst undertaking each of the EGR rate sweeps, fuel injection quantity and fuel injection timing were maintained constant. As the EGR valve was opened, changes in boost pressure were compensated for by adjusting the variable geometry turbocharger guide vane angle – this delivers EGR by reducing the fresh air charge. Figure 5 shows the maximum EGR rate that can be achieved within the EGR region. The maximum EGR rate was determined based on the effect of EGR on Hydrocarbon (HC) and carbon monoxide (CO) emissions: the limiting EGR rate was determined as the point at which HC or CO had increased by more than 300% compared to the zero EGR case or the point at which EGR flow could not be increased without a drop in intake manifold pressure. Points in Figure 4 without EGR were also identified by the same criteria.

4.2. Instrumentation and measurements

The engine was monitored by two data acquisition systems: the first was a *CP Engineering Cadet Automation System* monitoring low frequency data at a rate of 20Hz and the second was a *D2T Osiris* system capturing indication data for every 0.1°CA. Table 2 summarizes the key instrumentation used in this study.

Table 2: Summary of key Instrumentation sensors

Low frequency	CP Engineering Cadet Automation system			
Channel	Sensor	Range	Accuracy	
Fuel Flow	CP FMS1000 Gravimetric Flow Meter	0-300kg/h	+/-0.05%(a)	
Air Flow	ABB Sensy flow FMT700-P hot wire flow meter	0-800kg/h	+/-1%	
Gas Pressure	Piezo-resistive pressure transducers	0-5bar(b)	+/-10kPa	
Gas Temperature	k-type thermocouple 1.5mm	0-1200K	+/-2.2°C	
Engine Torque	HBM analogue torque sensor	-500-500Nm	0.05%	
CO ₂ Emissions concentrations	Horiba Mexa 7000 Analyser	0.5-20%vol	2% ^(c)	

High Frequency	D2T Osiris System		
Channel	Sensor	Range	Accuracy
In-cylinder pressure	Kistler Piezoelectric Pressure Sensor (Type 6056A) installed in glow plug adaptor	0-250bar	+/-2%(d)
Fuel rail pressure	Kistler Piezoelectric Pressure sensor (Type 4067A) installed on rail supply pipe	0-2000bar	+/-0.5%
Injector current	Pico Technology TA009 current clamp	10mA-20A	+/-2%+/-5mA

⁽a) Does not include installation effects which can affect the accuracy of measuring fuel consumed using gravimetric flow meters [74]

The EGR rate was determined by two measurements of CO_2 volumetric concentration, the first taken in the exhaust flow ($CO_{2,exh}$)just after the turbocharger turbine and the second taken from the intake manifold ($CO_{2,inl}$). Both volumetric concentrations are converted into mass concentrations according to equation 21.

$$Y_{CO_2,i} = \frac{\dot{m}_{CO_2,i}}{\dot{m}_i} = K_{dw} \ u_{CO_2} C_{CO_2,i}$$
 21

Where C_{CO_2} is a volumetric concentration measured by the emissions analysers, i represents either inlet of exhaust manifolds, u_{CO2} is a constant and K_{dw} is a correction factor to account for the fact that the emissions analyser removes water vapour before measuring the CO volumetric concentration [75].

⁽b) Range of pressure transducers used to measure intake manifold and exhaust manifold pressures.

⁽c) Emissions analyser accuracy achievable with daily calibration

⁽d) Accuracy for in-cylinder pressure measurement does not include the accuracy of pressure pegging (i.e. determining absolute values). This accuracy is the accuracy of the sensor which measures change in pressure over time and includes drift due to thermal shock

EGR mass airflow was calculated by applying a CO₂ balance as shown in equation

$$(\dot{m}_{air} + \dot{m}_{EGR})Y_{CO_2,inl} = \dot{m}_{air}Y_{CO_2,air} + \dot{m}_{EGR}Y_{CO_2,exh}$$
 22

Assuming the CO_2 concentration in the fresh intake air, $Y_{CO2,air}$, is negligible, then the EGR mass flow can be obtained from the two CO_2 concentrations and the measured intake air flow according to equation 22.

$$\dot{m}_{EGR} = \frac{Y_{CO_2,inl} \dot{m}_{air}}{Y_{CO_2,exh} - Y_{CO_2,inl}}$$
 23

EGR fraction can then be found as a function of $\dot{m}_{\it EGR}$ and $\dot{m}_{\it air}$, as show in equation 24.

$$\chi_{EGR} = \frac{\dot{m}_{EGR}}{\dot{m}_{air} + \dot{m}_{EGR}}$$
 24

4.3. Determining Measured Combustion Parameters

Measured indicated data was pre-processed to allow comparison model. Raw pressure data was collected for 100 consecutive engine cycles and the following data processing steps were taken before computing the combustion parameters:

- An angle based arithmetic average of the 100 cycles was calculated to remove random noise.
- A double-spline low-pass filter [76] was applied to smooth systematic noise in the pressure trace. This noise largely consists of high frequency pressure oscillations caused by the high rate of pressure rise during pre-mixed combustion, but also includes noise caused by the inlet and exhaust valve movements.
- The absolute magnitude of pressure was pegged by assuming the pressure rise during compression to be polytropic and using the two-point method with fixed polytropic index [77].

The measured pressure trace was aligned with the calculated cylinder volume by identifying the location of top dead centre through a motored pressure trace and inclusion of thermodynamic offset [78].

The raw pressure trace was subsequently used to calculate the observed combustion rate of heat release based on equation 1. In this analysis, the combustion heat release curve is the unknown with each of the other terms being known or modelled as follows:

- The internal energy term was estimated from the in-cylinder temperature, calculated from the measured cylinder pressure and the perfect gas law. The in-cylinder trapped mass was estimated using a filling and emptying model, the rate of fuel injection and blow-by [79]. For heat release calculation, the fuel injection rate was assumed to be constant for the injection duration and vaporization was ignored. Blow-by flow was estimated as an isentropic discharger through a nozzle [44]. The cumulative blow-by estimated by this model was validated using a Labcell M400MR Bow-By Monitor (accuracy +/-1.5%).
- The heat transfer term was modelled using the model proposed by Finol [70]
- The work term is calculated from the in-cylinder pressure and calculated cylinder volume [31].
- The intake and exhaust enthalpies were calculated based on the filling and emptying model and the in-cylinder temperature [80] and the blow-by enthalpy from blow-by flow using instantaneous nozzle model [71].

Using the processed in-cylinder pressure measurement, the calculated rate of heat release and a measurement of cylinder pressure from a motored cycle, the following quantities were calculated as followed:

Ignition delay was calculated as the time between start of injection and start of combustion. Start of injection was estimated based on measured current in the injector solenoid and a model of the injector hydraulics to account for needle lift delay. Start of combustion was determined differently for pilot and main injections:

- For pilot injection was determined by considering the second differential of in-cylinder pressure [68, 81]
- For main injection was determined by assessing when the calculated rate of heat release increased above a significant threshold. For high loads where pilot and main combustion overlap, a Wiebe model was fitted to the main combustion event to predict the start of main combustion.

Peak heat release rate, angle of peak heat release, peak pressure and angle of peak pressure were identified directly from the calculated heat release rates and processed pressures. The detailed uncertainty of each of these parameters is a complex topic and the focus of research in its own right, however a detailed sensitivity analysis performed by the authors has estimated the parameter accuracies in Table 3.

Table 3: Estimated combustion metric measurement accuracy [75]

Output	<i>IMEP</i>	$dQ_{c,max}$	Q_c	SOC	QHT
Predicted error	±1.1%	±4.9%	±1.4%	±0.29°CA	±12.2%

4.4. Model Parameterisation

For the simulation of all operating points, measured pressures in the intake and exhaust manifolds were imposed as well as measured temperature of the fresh air at the intercooler outlet (prior to mixing with the EGR flow). The cylinder wall temperature was also imposed based on cylinder temperature measurements [82]. For each condition, the simulated EGR valve opening was determined to match the measured cycle-averaged the fresh air flow.

The model was fitted using a single set of model parameters applied to all engine operating points. The parameterisation of the model was undertaken in a series of sequential steps which are detailed in figure 6. For each step in the identification, the targets model coefficients are highlighted from the model equations described in section 3. The experimental points used for the identification are also

shown and refer to the points in figure 4. The ignition delay can be measured directly from the incylinder pressure and the model prediction of ignition delay is not dependent on any other combustion sub-models; therefore, this model was parameterised first. A manual adjustment of the parameters was then necessary to achieve a sensible model output. This manual adjustment was based on information available in the literature and a trial and error approach. The next three steps provided the fine tuning of parameters for the diffusion and pre-mixed combustion. This process was performed iteratively as each model will influence the other when comparing the ability to match the measured rate of heat release. This iterative process was performed at operating points where wall impingement was unlikely and EGR was disabled. The final two steps then corresponded to the wall impingement and EGR model training.

Optimization of the model parameters was performed using the MATLAB algorithm 'fminsearch', which minimizes the target function for a given set of coefficients. The optimisation target was different depending on the step in figure 6. The stopping criteria for the fitting algorithm was a convergence criterion whereby the model fit did not improve by more than a minimum threshold with each loop.

5. Results and discussion

Table 4 summarises the correlations of measured and modelled combustion parameters for test points with and without EGR. Most of the fit statistics without EGR have an R² value in the region of 0.99. In section 5.1 these results will be explored in more details, analysing the fit over the engine operating range. For tests with EGR, the model performs well in predicting in-cylinder pressure but struggles with the combustion metrics. In section 5.2 these results will be explored in further detail to understand the observed model performance.

 $Table\ 4-Comparison\ of\ model\ correlation\ coefficients\ (R^2)\ for\ RoHR\ data\ with\ EGR,\ and\ without\ EGR$

Parameter	Without EGR	With EGR
p_{max}	0.989	0.946
$\theta_{max,RoHR}$	0.744	0.516
$ heta_{SOC,main}$	0.998	0.768
$RoHR_{max}$	0.961	0.323
$IMEP_{gross}$	0.996	0.990

1

2

3

6

9

10

11

12

13

14

15

16

17

18

19

20

5.1. Base Combustion model without EGR

5.1.1. Rate of heat release prediction

Figure 7 compared measured and modelled rate of heat release for 12 different engine operating points without EGR. The model can capture both shape and magnitudes and the strongest points are:

- 1. Ignition delay and its effect on initial pre-mixed for operating points with a large proportion of pre-mixed combustion (points a, b and e).
- 2. Combustion decay after the end of injection these are high load points with long injection durations and significant diffuse combustion (points g, h, k and l).
- 3. The end of combustion for low load points where the combustion is mainly pre-mixed and the end of combustion is dominated by the dynamics of the flame front (points a to d).
- 4. The effects of wall impingement which reduce peak heat release rates at full load conditions (points i to l).
- 5. The magnitude and phasing of pilot combustion for most operating points.

Weaker model performance was observed for the following conditions:

- Pre-mixed combustion at high engine speeds (points d, h and l) which could have been caused by using a low speed operating point to parameterise the pre-mixed combustion model
- 2. Pilot combustion at where pilot quantity is small (points d, h and j), as a result the main combustion appears greater because fuel injected during the pilot injection is added to the fuel at the onset of combustion.

5.1.2. Ignition Delay

Figure 8 compares measured and predicted ignition delay for the main injection event. The graphs are grouped by engine speed and plotted against rail pressure which captures the increase in indicated torque, therefore higher rail pressure in this representation corresponds approximately to higher engine load. The ignition delay model, which is also affected by pilot injection and ignition, performs well for speeds above 2000rev/min (Figure 8 c to f). The model is worse at lower engine speeds and most markedly at 1000rpm (Figure 8a). This is the most challenging point for the cylinder filling and emptying model which leads to poor estimation of in-cylinder mass, pressure and crucially temperature. An underestimation of the cylinder temperature would cause the over-estimation of ignition delay. There is also more uncertainty in the measured start of combustion at highest and lowest speeds and low engine loads because it becomes difficult to distinguish between the main and pilot burn.

5.1.3. Peak Heat Release

The measured and modelled maximum heat release rates are compared on figure 9. The peak heat release rate increases with BMEP at all engine speeds and this trend and magnitude is correctly captured. The poorest agreement occurs at 3500rpm where these is an underestimate in overall magnitude.

5.1.4. Point of peak heat release

Figure 10 compares measured and modelled angle of peak in-cylinder pressure. Despite the low R² value in table 4, the model qualitatively captures the trends and magnitudes, including the discontinuities between low and high loads at 1500rpm and 2500rpm. The most notable exception is at low load condition at 3000rpm (figure 10e). Considering the detailed plot of heat release rate for low load at 3000rev/min in figure 7c, this is explained by an overestimation of main combustion heat release rate.

5.2. Extended combustion model with EGR

5.2.1. Ignition delay

Figure 11 shows experimental and simulated ignition delay for the main injection. The model correctly predicts the trend of increased ignition delay with increased EGR rate. The model also reflects the interactions with engine speed and load which reduce the effect of EGR due to higher magnitudes of fresh air flow and fuel energy. One notable exception is the condition at 1500rpm and 100Nm where the model substantially over-predicts the impact of EGR due to the under-prediction of cylinder pressure and temperature prior to the main combustion event.

In many of the test points there is an offset between the experimental and predicted data, even for low EGR rates. This suggests that this error is not a response to the EGR modelling, but rather to another variable that affects the ignition delay sub-model. Small errors in-cylinder mass and temperature can have a large influence on ignition delay, and it is likely that assumptions made in the filling and emptying model and the heat transfer model will contribute to overall error. Mixing within the inlet manifold was assumed to be perfect, and cylinder-to-cylinder variations were ignored. In addition, cycle-to-cycle variation will result in discrepancies between time-averaged and cycle-averaged data, both of which are model inputs and model validation metrics.

The prediction of pilot affects pressure and temperature history prior to main injection and influences main injection ignition delay. In several cases, pilot combustion was over-predicted by up to 300%: Figure 12 shows an example of such a case. Overestimating the pilot combustion affects the main combustion in two ways:

- The temperature and pressure in the cylinder are higher (more energy release). This tends to shorten the ignition delay for the main injection as per equation 6. The shorter ignition delay leads to less fuel combusting in the pre-mixed mode
- There is less unburned fuel, injected but not burnt during the pilot injection that will subsequently burn in the main combustion event.

The difference in pilot prediction is thought to be due to the very early injection timing employed when EGR is enabled. It is hypothesised that this leads to the pilot combustion leaning out due to excess air before all the fuel has been consumed, since this was observed even with very low concentrations of EGR. The ignition delay for main injection would increase because the temperature rise from pilot injection is reduced and it is possible that the unburnt fuel from the pilot then contributes to the main combustion event. Both will increase the main pre-mixed spike as seen in the measured data (see Figure 12). Since the model assumes a fixed stoichiometric ratio (λ) for pilot combustion, it is not possible for the current simulation to model this behaviour. In addition, the effect of EGR on pilot combustion would be magnified compared to the effect on main combustion due to small amount of fuel and long ignition delay, reducing peak heat release rates further.

5.2.2. Peak RoHR

Figure 13 compares modelled and measured maximum heat release rate for different EGR rates and speed load points. Overall, the prediction for peak heat release rate is relatively poor compared to the other combustion metrics. This is especially true for low loads where there are large offsets between the measured and predicted data. For medium to high loads, the model offers better prediction. However, at these test points, the effect of EGR is reduced significantly because the EGR rates are lower and the charge densities higher.

This split between low-load and high-load conditions can be explained by the dominance of pre-mixed combustion. At low loads a greater portion of the fuel mass is dedicated to the pre-mixed model, since there is significantly more ignition delay at this point. This effect is amplified by the presence of EGR, which retards the SOC further and increases the pre-mixed portion. Although the trend in ignition delay was predicted well, there were significant offsets between the predicted and measured data (Figure 11). At low loads, the peak heat release rate is very sensitive to the amount of fuel dedicated to the pre-mixed model, and therefore also to the ignition delay: small errors in ignition delay can cause a large model errors. In some cases, it appears as if there is a greater amount of pre-mixed

combustion than would be predicted, even if the model predicted the SOC correctly. In these cases, it is theorised that a greater fraction of fuel injected during the ignition delay should have been dedicated to the pre-mixed combustion model, due to the presence of EGR and partially burnt pilot. Detailed assessment of the model presented by Rether et al. [39] shows the inclusion of varying excess air ratio during the pilot injection could improve the simulation at low load.

5.2.3. Point of peak RoHR

1

2

3

5

6

7

8

9

10

11

12

13

14

15

16

17

18

19

20

21

22

23

24

25

The point of peak RoHR ($\theta_{max,RoHR}$) is a useful metric of combustion phasing because it is a function of both ignition delay and RoHR. These results are plotted in figure 14. The trend of $\theta_{max.RoHR}$ increasing with additional EGR is predicted well by the model. In addition, the magnitude of $heta_{max.RoHR}$ is predicted well with some offsets observed particularly around mid-load points. In most cases, the offsets can be attributed to poor ignition delay prediction; however, the results for 2500rpm and 3000rpm, 100Nm load can be attributed to the model not predicting diffusion combustion correctly. Figure 15 shows an example of early prediction of peak RoHR: the measured data clearly exhibits two distinct peaks; the first being the pre-mixed event, and the second the peak diffusion event. The RoHR prediction is reasonable up to the first peak, showing that the differences can be attributed to the diffusion model. In the model, the RoHR is proportional to the available fuel mass and rate of injection, so at the EOI there is an exponential decay in RoHR. What this data implies is that either the rate of injection is over-predicted for this test point, or that there is another mechanism which is delaying the diffusion burn. It was assumed that the time for the fuel to reach the flame sheet was negligible, and that the kinetic energy density is proportional to the needle lift. In [46], it was suggested that there should be a time lag proportional to the injection rate to account for the time for fuel energy to reach the flame sheet. Since EGR increases the injection delay, and combustion occurs over an increased volume, the diffusion flame sheet is further away from the injector. This means the time delay becomes more significant, resulting in the phenomenon observed. The low R^2 for $\theta_{max,RoHR}$ presented in table 4 could have been caused by operating point offsets, which were due to poor SOC

prediction, since the trends with increasing EGR rate appear to be captured as explained in Section 5.2.3.

5.3. Summary of future model improvements

The shortfalls of the model with respect to EGR have been touched upon through the results analysis. These relate to all three of the combustion phases: pilot, pre-mixed and diffusion. The results suggested that pilot combustion was overpredicted when with the presence of EGR and this suggests that the influence of EGR on the pilot model should be increased. In particular, the model needs to be more sensitive to temperature and mixing and to have the ability stop the pilot combustion. This could be achieved by tuning the stoichiometric ratio (λ in equation 3) without EGR and whilst it offers simplicity, data from the EGR tests could be used to add mathematical flexibility to improve the prediction.

In some operating points the premixed combustion is underestimated with EGR. This problem could be solved by adjusting the amount of fuel partaking in the premixed combustion phase. This could either be achieved by varying the stoichiometric ratio for premixed combustion (λ in equation 3) or the amount of fuel dedicated to premix combustion (x_{pre} in equation 4). As for pilot, these two terms were paramterised without EGR and maintained constant for all operating points. Some dependency on EGR could be introduced to these terms. This would again increase the complexity of the model in exchange for potential benefits in accuracy.

For the diffusion combustion, a time lag to account for the fuel reaching the flame sheet could be added. This would need to be incorporated in the expression for $m_{f,diff,avail}$ (equation 9). In practive, this time lag would be a function of the velocity of the fuel injected into the cylinder (linked to rail pressure) and the size of the flame. As the flame will be larger in the presence of EGR, this term could be set as a function of EGR rate or in-cylinder concentration.

Each of these proposed model modifications would increase the number of parameters that need to be identified and therefore increase the empirical aspects of the model. Ultimately each individual application would need to trade-off this aspect depending on the available training data and modelling targets.

6. Conclusions

A Mixed Controlled Combustion model had been presented including enhancements for wall impingement, pre-mixed combustion, pilot combustion and EGR. The model was parameterised using a small set of selected engine operating points. Initially the combustion model parameters were identified without EGR and the resulting model predicted Rate of heat release, start of combustion, peak pressure, and combustion phasing with R² values above 0.95 across the complete engine operating map.

From the base model, the EGR parameters were identified using specific EGR test points and validated using measured EGR swings over the engine's EGR operating envelope. The R² values comparing simulation and measured results for the same combustion parameters were all reduced over the EGR operating region. However, close examination of results shows that most trends were captured well. Key errors in the pilot combustion were identified that have knock on effect onto the main combustion phasing and peak rates. However, despite these differences, the in-cylinder pressure was well predicted.

Pilot combustion was found to be over-predicted, since the pilot timing was early compared to conditions without EGR, resulting in pilot combustion leaning out and contributing to the main combustion. A more complex pilot model which considers the pilot λ to be variable, and could pass fuel between the pilot and main combustion models, would be required to simulate this effect accurately.

Peak heat release prediction was found to be relatively poor; however, this was mainly due to large offsets observed at the constant speed/load test points, rather than the correlation with change in EGR rate. Peak rates were affected, especially at low loads where combustion is mainly pre-mixed and most reliant on the SOC being correct, since SOC defines the portion of fuel dedicated to the pre-

mixed model. Also, it is suggested that partially burnt pilot may have contributed to the increased heat release rates during the initial pre-mixed burnt at low loads.

7. Notation

AFR_{stoich}	Stoichiometric air fuel ratio	
a_{1-4}	Model fitted parameters	
C_{arr}	Arrhenius model constant (Fitted)	
C_{CO_2}	Volumetric concentration of CO2	%
C_{evap}	Fuel Evaporation model constant	
C_{mag}	Magnussen model constant (Fitted)	
C_{mod}	Chmela diffusion Combustion model constant (fitted)	J/kg °CA
C_p	Specific heat capacity at constant pressure	J/kgK
C_V	Specific heat capacity at constant volume	J/kgK
d_{noz}	Injector Nozzle diameter	m
$IMEP_{gross}$	Gross Indicated mean effective pressure	Pa
Н	Enthalpy	J
h	Specific enthalpy	J/kg
K_{dw}	Dry/wet correction factor for CO2 emissions measurement	
k	Turbulence density	m^2/s^2
LCV	Lower Calorific Value of fuel	J/kg
m	mass	Kg
N_{eng}	Engine Speed	Rev/min

p	pressure	Pa
Q_C	Heat energy from combustion	J
Q_{HT}	Heat transfer through cylinder walls	J
R	Gas constant	J/kgK
R^2	Coefficient of Determination	
SOC	Start of Combustion	°ATDC
Т	Temperature	K
T_a	Fuel Activation Temperature	K
t	time	S
U	Internal energy	J
u_{CO2}	Relative density constant for CO2 emissions measurement	
V	Volume	m^3
W	Work	J
x	Proportion of fuel	
Y	Mass fraction	
γ	Ratio of specific heats	
θ	Crank Angle	o
λ	Stoichiometric ratio for premixed combustion	
ρ	density	Kg/m ³
τ	Delay time constant	s ⁻¹
χ_{EGR}	Fraction of EGR by mass	

Fresh air air Available fuel avail b Burnt gases Blow-by flow bb CO_2 Carbon Dioxide Chemical Ignition delay chdiffDiffusive combustion cylIn-cylinder Exhaust gas recirculation *EGR* Flow through exhaust valves exhfuel f IDIgnition Delay Injected inj inlFlow through intake valves

main Main injection or combustion event

max Peak/maximum

Liquid

liqu

ph Physical ignition delay

pre Pre-mixed combustion

soc Start of combustion

SOI Start of Injection

1

ATDC After top dead centre

BMEP Brake Mean Effective Pressure

CA Crank Angle

CO₂ Carbon dioxide

EOI End of Injection

HiL Hardware in the Loop

MCC Mixing Controlled Combustion

NO_x Oxides of nitrogen

RoHR Rate of Heat Release

SOC Start of Combustion

SOI Start of Injection

SSE Sum Squared Error

TDC Top dead centre

References

8.

2

3

5

7

8

9

1. Taylor AMKP. Science review of internal combustion engines. Energy Policy. 2008;36(12):4657-67.

2. Millet, J., Aubertin, F., Saad, C., Lehr, M. et al., "Air System and Diesel Combustion Model for a 4 Cylinder Engine in Real Time Computing Conditions: Application on a EU5 Personal Car with Diesel Particulate Filter," SAE

Technical Paper 2009-24-0136, 2009, doi:10.4271/2009-24-0136.

 Aithal SM. Impact of EGR fraction on diesel engine performance considering heat loss and temperaturedependent properties of the working fluid. International Journal of Energy Research. 2009;33(4):415-30.

1	4.	Macek, J., Vítek, O., Srinivasan, S., and Tanner, F., "1-D Modeling of Transient Engine Operations Using Data
2		Generated by a CFD Code," SAE Technical Paper 2008-01-0357, 2008, doi:10.4271/2008-01-0357.
3	5.	Engelmayer M, Wimmer A, Pirker G, Pemp B, Hirschl G. Simulation Based Development of Combustion Concepts
4		for Large Diesel Engines. ASME. Internal Combustion Engine Division Fall Technical Conference, ASME 2011
5		Internal Combustion Engine Division Fall Technical Conference ():75-83. doi:10.1115/ICEF2011-60194.
6	6.	Asad U, Zheng M. Real-time Heat Release Analysis for Model-based Control of Diesel Combustion, SAE
7		International; 2008, DOI: 10.4271/2008-01-1000, SAE Paper Number 2008-01-1000.
8	7.	Woermann, R. J., Theuerkauf, H. J. and Heinrich, A., A Real-Time Model of a Common Rail Diesel Engine, 1999,
9		SAE International, Warrendale, USA, DOI: 10.4271/1999-01-0862, SAE Paper Number 1999-01-0862
10	8.	Fiorani P, Gambarotta A, Tonetti M. and Lanfranco E., A Real-Time Model for the Simulation of Transient
11		Behaviour of Automotive Diesel Engines, SAE International; 2006, DOI: 10.4271/2006-01-3007, SAP paper
12		number 2006-01-3007
13	9.	Al-Durra A, Canova M. and Yurkovich S., A model-based methodology for real-time estimation of diesel engine
14		cylinder pressure. Journal of Dynamic Systems, Measurement and Control, Transactions of the ASME.
15		2011;133(3), DOI: 10.1115/1.4003370
16	10.	Kao M, Moskwa JJ, editors. Turbocharged diesel engine modeling for nonlinear engine control and state
17		estimation, Proceedings of the 1993 ASME Winter Annual Meeting, November 28 - December 3, 1993; 1993; New
18		Orleans, LA, USA: Publ by ASME
19	11.	Jensen JP, Kristensen AF, Sorenson SC, Houbak N and Hendricks E., Mean Value Modeling of a Small
20		Turbocharged Diesel Engine, SAE International Warrendale Pennsylvania USA: Detroit, Michigan, SAE Paper
21		Number 910070
22	12.	Müller M, Hendricks E and Sorenson SC., Mean Value Modelling of Turbocharged Spark Ignition Engines, 1998,
23		SAE International Warrendale Pennsylvania USA: Detroit, Michigan, SAE Paper Number 980784
24	13.	Fons M, Muller M, Chevalier A, Vigild C, Hendricks E and Sorenson SC., Mean Value Engine Modelling of an SI
25		Engine with EGR, 1999, SAE International Warrendale Pennsylvania USA: Detroit, Michigan., SAE Paper Number
26		1999-01-0909
27	14.	He Y and Lin C-C., Development and Validation of a Mean Value Engine Model for Integrated Engine and Control
28		System Simulation, 2007, SAE International Warrendale Pennsylvania USA: Detroit, Michigan, SAE Paper Number
29		2007-01-1304
30	15.	Lee B and Jung D., Thermodynamics-based mean-value engine model with main and pilot injection sensitivity,
31		Proceedings of the Institution of Mechanical Engineers, Part D: Journal of Automobile Engineering.

2016;230(13):1822-34, DOI: 10.1177/0954407015624525

9

10 11

13

14

12

15 16

17 18

19 20

21

22 23

24 25

27

26

28 29

30

- 16. Andersson M, Johansson B, Hultqvist A and Nöhre C., A Real Time NOx Model for Conventional and Partially Premixed Diesel Combustion, SAE International; 2006, 10.4271/2006-01-0195, SAE Paper Number 2006-01-0195
- 17. D'Ambrosio S, Finesso R, Fu L, Mittica A and Spessa E. A control-oriented real-time semi-empirical model for the prediction of NOx emissions in diesel engines, Applied Energy. 2014, pp. 130:265-79., DOI: 10.1016/j.apenergy.2014.05.046
- 18. Karaky, H., Mauviot, G., Tauzia, X., and Maiboom, A., "Development and Validation of a New Zero-Dimensional Semi-Physical NOx Emission Model for a D.I. Diesel Engine Using Simulated Combustion Process," SAE Int. J. Engines 8(4):1924-1937, 2015, doi:10.4271/2015-01-1746.
- 19. Poetsch, C. and Katrasnik, T., "Crank-Angle Resolved Modeling of Fuel Injection, Combustion and Emission Formation for Engine Optimization and Calibration on Real-Time Systems," SAE Technical Paper 2016-01-0558, 2016, doi:10.4271/2016-01-0558.
- 20. Asprion J, Chinellato O, Guzzella L. A fast and accurate physics-based model for the NOx emissions of Diesel engines. Applied Energy. 2013;103:221-33.
- 21. Karaky, H., Mauviot, G., Tauzia, X., and Maiboom, A., "Semi-Empirical OD Modeling for Engine-Out Soot Emission Prediction in D.I. Diesel Engines," SAE Technical Paper 2016-01-0562, 2016, doi:10.4271/2016-01-0562.
- 22. Maiboom A. Etude Experimentale et modelisation phenomenologique de l'influence des characteristiques thermodynamiques et de la compression des gaz d'admission sur la combustion et les emissions d'un moteur Diesel automobile. (PhD Thesis): Ecole Centrale Nantes; 2007.
- 23. Maiboom A, Tauzia X, Shah SR, Hetet J-F. New phenomenological six-zone combustion model for direct-injection diesel engines. Energy and Fuels. 2009;23(2):690-703.
- 24. Rajkumar S, Sudarshan G. Multi-zone phenomenological model of combustion and emission characteristics and parametric investigations for split injections and multiple injections in common-rail direct-injection diesel engines. Proceedings of the Institution of Mechanical Engineers, Part D: Journal of Automobile Engineering. 2015;229(10):1310-26.
- 25. Liu L, Horibe N, Ishiyama T. Combustion modelling for a diesel engine with multi-stage injection using a stochastic combustion model. Proceedings of the Institution of Mechanical Engineers, Part D: Journal of Automobile Engineering. 2014;228(5):518-34.
- 26. Nishida K., Hiroyasu H., "Simplified Three-Dimensional Modelling of Mixture Formation and Combustion in a D.I. Diesel Engine", SAE paper no. 890269, pp. 276-293, 1989
- 27. Hiroyasu H., Kadota T., Arai M., "Development and Use of a Spray Combustion Modeling to Predict Diesel Engine Efficiency and Pollutant Emissions", bulletin of the JSME, Vol. 26, no. 214, 1983

1	2	28.	Grill, M., Bargende, M., Rether, D., and Schmid, A., "Quasi-dimensional and Empirical Modeling of Compression-
2			Ignition Engine Combustion and Emissions," SAE Technical Paper 2010-01-0151, 2010, doi:10.4271/2010-01-
3			0151.
4	2	19.	Gao Z, Wagner RM, Sluder CS, Daw CS, Green Jr JB. Using a phenomenological computer model to investigate
5			advanced combustion trajectories in a CIDI engine. Fuel. 2011;90(5):1907-18.
6	3	80.	Bittle JA, Gao Z, Jacobs TJ, editors. Validation and results of a pseudo-multi-zone combustion trajectory
7			prediction model for capturing soot and nox formation on a medium duty diesel engine. ASME 2013 Internal
8			Combustion Engine Division Fall Technical Conference, ICEF 2013, October 13, 2013 - October 16, 2013; 2013;
9			Dearborn, MI, United states: American Society of Mechanical Engineers (ASME).
10	3	31.	Heywood, J.B., Internal Combustion Engine Fundamentals1988, New York: McGraw-Hill.
11	3:	32.	Pacitti G, Amphlett S, Miller P, Norris R, Truscott A. Real-Time Crank-Resolved Engine Simulation for Testing New
12			Engine Management Systems, 2008, DOI: 10.4271/2008-01-1006, SAE Paper Number: 2008-01-1006
13	3.	3.	Gao Z, Schreiber W. A phenomenologically based computer model to predict soot and NOx emission in a direct
14			injection engine. Int J Engine Res. 2001;2(3):177–88.
15	3	84.	Galindo J, Lujan JM, Serrano JR and Hernandez L., Combustion simulation of turbocharger HSDI Diesel engines
16			during transient operation using neural networks, Applied Thermal Engineering, 2005;25(5-6):877-98, DOI:
17			10.1016/j.applthermaleng.2004.08.004
18	3.	85.	Ponti F, Ravaglioli V, De Cesare M, editors. Development of a common rail diesel engine combustion model for
19			ROHR real-time estimation, ASME 2011 Internal Combustion Engine Division Fall Technical Conference, ICEF
20			2011, October 2, 2011 - October 5, 2011; 2011; Morgantown, WV, United states: American Society of Mechanical
21			Engineers, DOI: 10.1115/ICEF2011-60153
22	3	86.	Maroteaux F, Saad C, Aubertin F, Canaud P., Analysis of Crank Angle Resolved In-Cylinder Combustion Modelling
23			for Real Time Diesel Engine Simulations, SAE International; 2015, DOI: 10.4271/2015-24-2394, SAE Paper
24			Number: 2015-24-2394
25	3	37.	Saad C, Marteau F, Millet J-B, Aubertin F., Combustion Modeling of a Direct Injection Diesel Engine Using Double
26			Wiebe Functions: Application to HiL Real-Time Simulations, SAE International; 2011., DOI 10.4271/2011-24-0143,
27			SAE Paper Number: 2011-24-0143

38. Ponti, F., Ravaglioli, V., Moro, D., and Serra, G., "Common Rail Multi-Jet Diesel Engine Combustion Development

Investigation for MFB50 On-board Estimation," SAE Technical Paper 2010-01-2211, 2010, doi:10.4271/2010-01-

28

29

30

2211.

rate prediction in high-speed DI diesel engines with common-rail injection, SAE Paper Number 2000-01-2933, SAE

1		International Fall Fuels and Lubricants Meeting and Exhibition 2000, SAE International Warrendale Pennsylvania USA:
2		Baltimore, MD.
3	50	O. Finesso R, Spessa E, Yang Y, Alfieri V, Conte G., HRR and MFB50 Estimation in a Euro 6 Diesel Engine by Means of
4		Control-Oriented Predictive Models, 2015., DOI: 10.4271/2015-01-0879, SAE Paper Number: 2015-01-0879
5	5:	1. Finesso R. and Spessa E., Real-Time Predictive Modeling of Combustion and NOx Formation in Diesel Engines Under
6		Transient Conditions, SAE International; 2012., DOI: 10.4271/2012-01-0899, SAE Paper Number 2012-01-0899
7	52	2. Tauzia X, Maiboom A, Chesse P, Thouvenel N. A new phenomenological heat release model for thermodynamical
8		simulation of modern turbocharged heavy duty Diesel engines. Appl Therm Eng. 2006;26(16):1851-7.
9	53	3. Katranik T., An advanced real-time capable mixture controlled combustion model, Energy. 2016;95:393-403, DOI:
10		10.1016/j.energy.2015.11.066
11	54	4. Rezaei, R., Eckert, P., Seebode, J. and Behnk, K., "Zero-Dimensional Modeling of Combustion and Heat Release
12		Rate in DI Diesel Engines," SAE Int. J. Engines 5(3):2012, doi:10.4271/2012-01-1065
13	55	5. Lebas, R., Fremovici, M., Font, G., and Le Berr, F., "A Phenomenological Combustion Model Including In-Cylinder
14		Pollutants To Support Engine Control Optimisation Under Transient Conditions," SAE Technical Paper 2011-01-
15		1837, 2011, doi:10.4271/2011-01-1837.
16	56	6. Rudloff, J., Dulbecco, A., and Font, G., "The Dual Flame Model (DFM) : A Phenomenological 0D Diesel Combustion
17		Model to Predict Pollutant Emissions," SAE Technical Paper 2015-24-2388, 2015, doi:10.4271/2015-24-2388.
18	57	7. Ladommatos, N., Abdelhalim, S.M., Zhao, H. and Hu, Z., The dilution, chemical, and thermal effects of exhaust gas
19		recirculation on diesel engine emissions~Part 1: Effect of reducing inlet charge oxygen, in SAE International Spring
20		Fuels and Lubricants Meeting and Exposition 1996, SAE International Warrendale Pennsylvania USA: Dearborn,
21		Michigan. SAE Paper Number 961165
22	58	8. Ladommatos, N., Abdelhalim, S.M., Zhao, H. and Hu, Z., <i>The dilution, chemical, and thermal effects of exhaust gas</i>
23		recirculation on diesel engine emissions~Part 2: Effects of carbon dioxide, in SAE International Spring Fuels and
24		Lubricants Meeting and Exposition 1996, SAE International Warrendale Pennsylvania USA: Dearborn, Michigan. SAE
25		Paper Number 961167
26	59	9. Ladommatos, N., Abdelhalim, S.M., Zhao, H. and Hu, Z., <i>The dilution, chemical, and thermal effects on exhaust gas</i>
27		recirculation on diesel engine emissions~Part 3: effects of water vapor, in SAE International Spring Fuels and
28		Lubricants Meeting and Exposition 1997, SAE International Warrendale Pennsylvania USA: Dearborn, Michigan. SAE
29		Paper Number 971659

1			
2			
3			
4			
5			
6			
7			
8			
9			
10			
11			
12			
13			
14			
15			
16			
17			
18			
19			
20			
21			
22			
23			
24			
25			
26			
27			
28			
29			

60.	Ladommatos, N., Abdelhalim, S.M., Zhao, H. and Hu, Z., The dilution, chemical, and thermal effects of exhaust gas
	recirculation on diesel engine emissions~Part 4: effects of carbon dioxide and water vapor, in SAE International Spring
	Fuels and Lubricants Meeting and Exposition 1997, SAE International Warrendale Pennsylvania USA: Dearborn,
	Michigan. SAE Paper Number 971660

- 61. Ladommatos, N., Abdelhalim, S.M., Zhao, H. and Hu, Z., Effects of EGR on heat release in diesel combustion, in SAE International Congress and Exposition 1998, SAE International Warrendale Pennsylvania USA: Detroit, Michigan. SAE Paper Number 980184
- 62. Maiboom, A., Tauzia, X., Hetet, J-F., Cormerais, M., Yousni, M., Jaine, T. and Blanchin, S., *Various Effects of EGR on Combustion and Emissions on an Automotive DI Diesel Engine: Numerical and Experimental Study*, in *2007 JSAE/SAE International Fuels and Lubricants Meeting* 2007, SAE International Warrendale Pennsylvania USA: Kyoto, Japan, SAE Paper Number 2007-01-1834
- 63. Burke, R., C. Brace, and S. Akehurst. Engine and Combustion Stability over extended Operating Range using Engine

 Thermal Management in Calibration Procedure. in Diesel Engines, facing the competitiveness challenges. 2010.

 Rouen, France: SIA.
- 64. Arsie, I., Criscuolo, I., Pianese, C., and De Cesare, M., "Tuning of the Engine Control Variables of an Automotive Turbocharged Diesel Engine via Model Based Optimization," SAE Technical Paper 2011-24-0146, 2011, doi:10.4271/2011-24-0146.
- 65. Poetsch, C., "Crank-Angle Resolved Modeling of Fuel Injection and Mixing Controlled Combustion for Real-Time Application In Steady-State and Transient Operation," SAE Technical Paper 2014-01-1095, 2014, doi:10.4271/2014-01-1095.
- 66. Wurzenberger JC, Poetsch C., Plant Modeling for Closed Loop Combustion Control A Thermodynamic Consistent and Real-Time Capable Approach, SAE International; 2015., DOI: 10.4271/2015-01-1247, SAE Paper Number 2015-01-1247
- 67. Finol, C.F., Heat transfer investigations in a modern Diesel engine, PhD Thesis, 2008, Dept. of Mechanical Engineering,
 University of Bath, Bath
- 68. Assanis, D.N., Filipi, Z.S., Fiveland, S.B. and Syrimis, M., A predictive ignition delay correlation under steady-state and transient operation of a direct injection diesel engine, Journal of Engineering for Gas Turbines and Power-Transactions of the ASME, 2003. 125(2): p. 450-457.
- 69. Magnussen, B.F. and Hjertager, B.H., On mathematical modeling of turbulent combustion with special emphasis on soot formation and combustion. Symposium (International) on Combustion, 1977. 16(1): p. 719-729

1	70.	Dowell, P.G., Akehurst, S. and Burke, R.D., An Improved Rate of Heat Release Model for Modern High Speed Diesel
2		Engines, 2016, ASME Paper Number ICEF2016-9630, Proceedings of the ASME 2016 Internal Combustion Engine
3		Fall Conference, Oct. 9-12 2016, Greenville, SC, USA
4	71.	Lapuerta, M., Armas, O., and Hernandez, J.J., Diagnosis of DI Diesel combustion from in-cylinder pressure signal by
5		estimation of mean thermodynamic properties of the gas. Applied Thermal Engineering, 1999. 19 (5): p. 513-529.
6	72.	Dowell, P.D., Real time heat release model of a HSDI Diesel engine, PhD Thesis, 2012, Dept. of Mechanical
7		Engineering, University of Bath, Bath
8	73.	Zweiri, Y.H., Whidborne, J.F. and Seneviratne, L.D., Detailed analytical model of a single-cylinder diesel engine in the
9		crank angle domain. Proceedings of the Institution of Mechanical Engineers Part D-Journal of Automobile
10		Engineering, 2001. 215 (D11): p. 1197-1216.
11	74.	Burke, R. D., Brace, C. J. and Hawley, J. G., 2011. Critical evaluation of on-engine fuel consumption measurement.
12		Proceedings of the Institution of Mechanical Engineers, Part D: Journal of Automobile Engineering, 225 (6), pp.
13		829-844.
14	75.	N.d., BS ISO 8178-1:2006. Reciprocating internal combustion engines. Exhaust emission measurement. Test-bed
15		measurement of gaseous and particulate exhaust emissions, BSI.
16	76.	Zhong, L., Henein, N.A., and Bryzik, W., Effect of smoothing the pressure trace on the interpretation of experimental
17		data for combustion in diesel engines, in SAE 2004 World Congress and Exhibition 2004, SAE International Warrendale
18		Pennsylvania USA: Detroit, Michigan. SAE Paper Number 2004-01-0931
19	77.	Randolph, A.L., Methods of processing cylinder-pressure transducer signals to maximize data accuracy, in SAE
20		International Congress and Exposition 1990, SAE International Warrendale Pennsylvania USA: Detroit, Michigan, SAE
21		Paper Number 900170
22	78.	Marek, J.S., Thermodynamic determination of T.D.C. in piston combustion engines, in SAE International Congress and
23		Exposition1996, SAE International Warrendale Pennsylvania USA: Detroit, Michigan, SAE Paper Number 960610
24	79.	Schuette, H. and Ploeger, M., Hardware-in-the-Loop Testing of Engine Control Units~A Technical Survey, in SAE 2007
25		World Congress 2007, SAE International Warrendale Pennsylvania USA: Detroit, Michigan, SAE Paper Number 2007-
26		01-0500
27	80.	Schulten, P.J.M. and Stapersma, D., Mean value modelling of the gas exchange of a 4-stroke diesel engine for use in
28		powertrain applications, in SAE 2003 World Congress2003, SAE International Warrendale Pennsylvania USA: Detroit,
29		Michigan, SAE Paper Number2003-01-0219

1 81. Wurzenberger, J.C., Heinzle, R., Schuemie, A. and Katrasnik, T., *Crank-Angle Resolved Real-Time Engine Simulation* 2 *Integrated Simulation Tool Chain from Office to Testbed*, in *SAE 2009 World Congress* 2009, SAE International
3 Warrendale Pennsylvania USA: Detroit, Michigan, SAE Paper Number 2009-01-058

82. Lewis A.G., Akehurst S., Brace C.J., Finol C. and Robinson K., *Dynamic Measurement of Heat Flux through the Cylinder Wall of a Modern HSDI Engine Over a New European Drive Cycle*. SAE International; 2010, SAE Paper Number 2010-01-0322

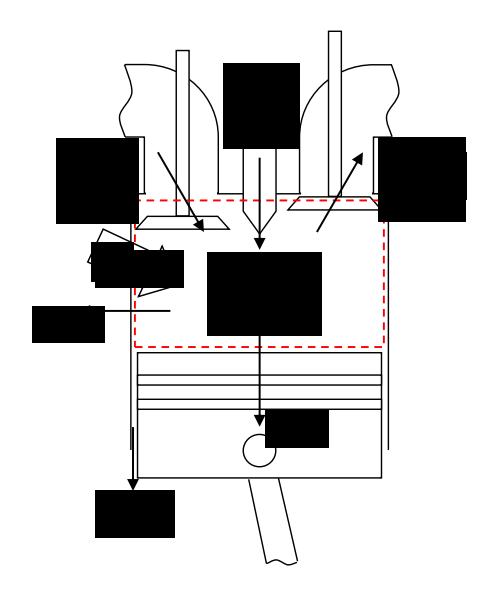


Figure 1: Combustion chamber control volume with mass and energy transfer for a single zone model

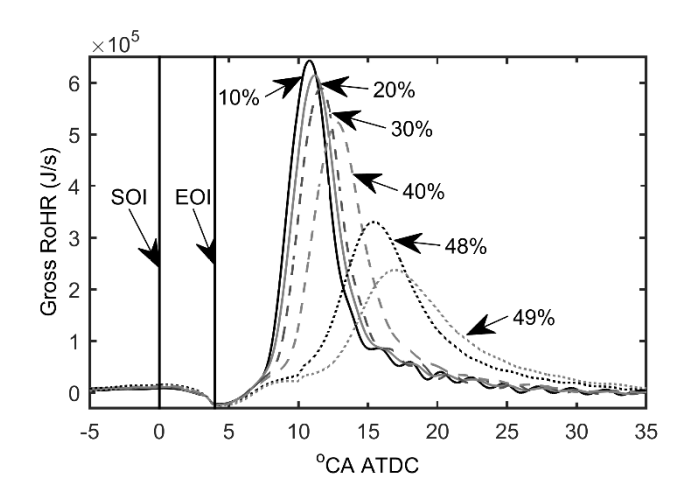


Figure 2: Effect of increasing percentage EGR on apparent heat release at 2000rev/min and 20Nm

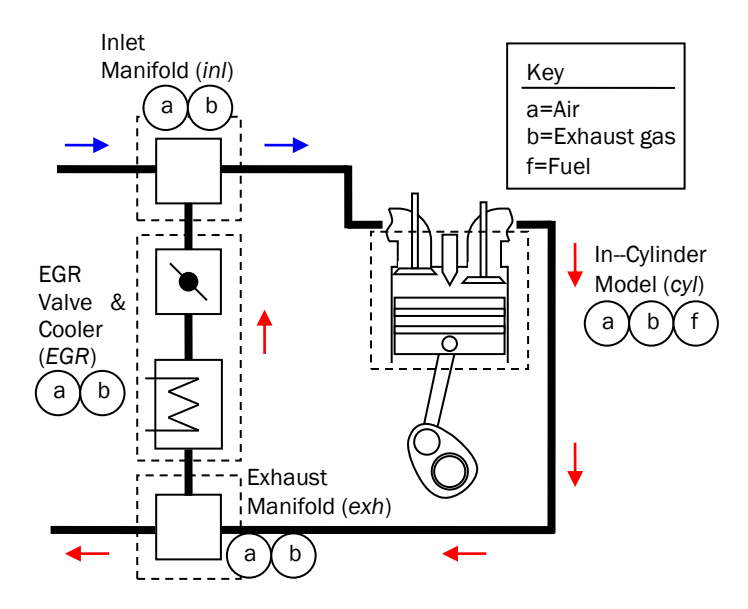


Figure 3: Layout of control volumes for air path model to estimate flows of EGR and cylinder gas composition

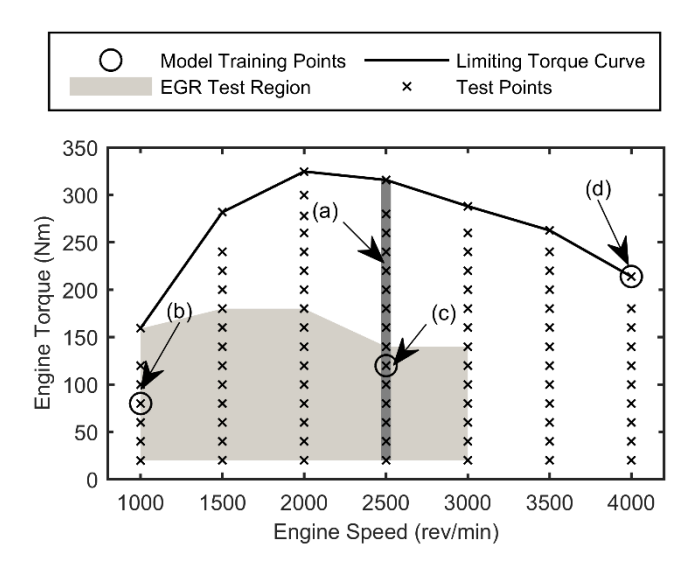


Figure 4: Engine speed/ torque map illustrating all test points used for model validation. Points used for model training are highlighted as: (a) diffusion combustion, (b) pre-mixed combustion, (c) ignition delay and (d) wall impingement

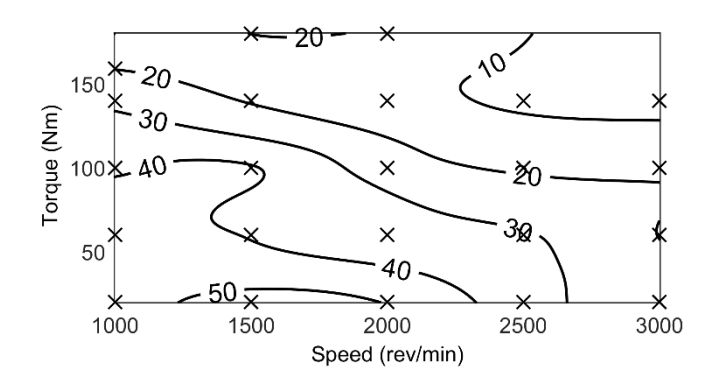
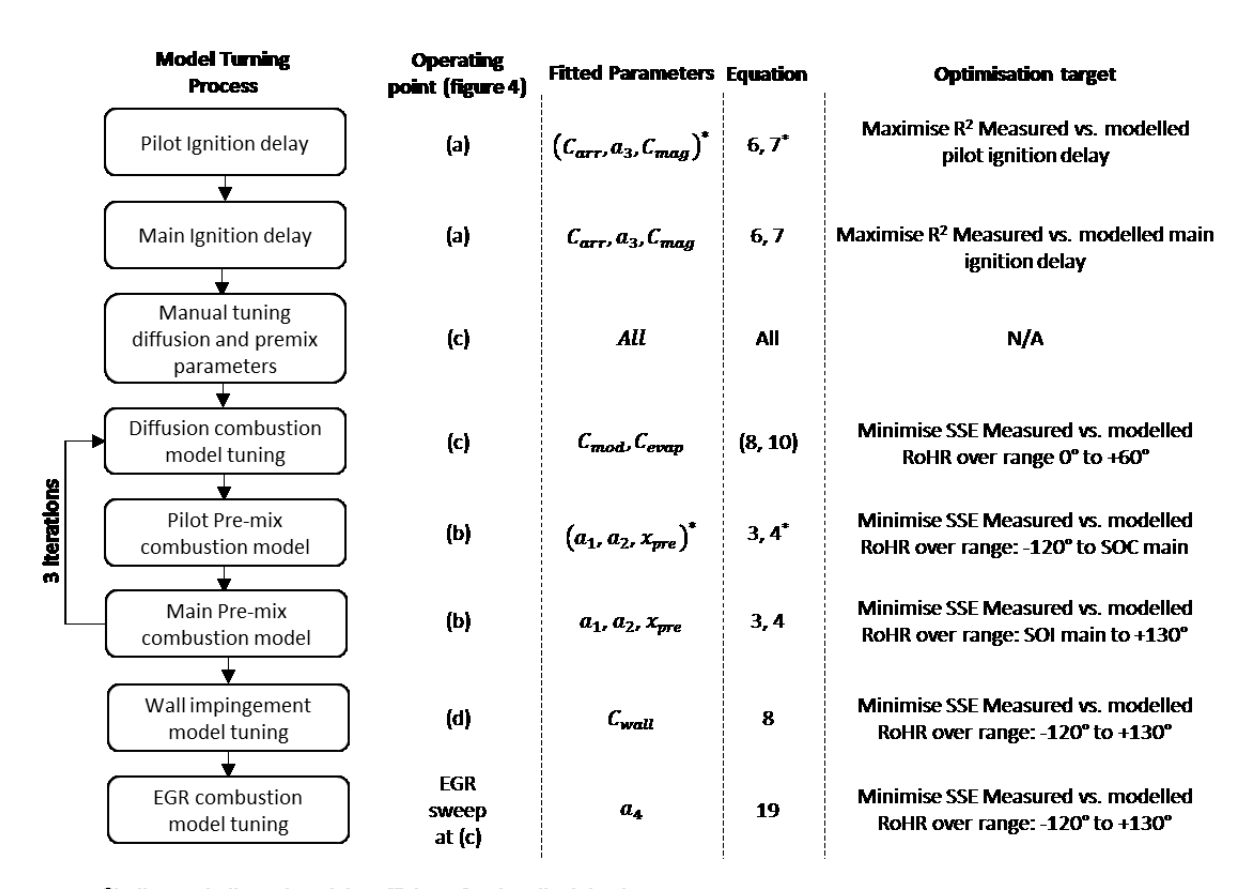


Figure 5: Maximum achievable EGR rates within the EGR test region



 $^{f *}$ indicates dedicated model coefficients for the pilot injection

RoHR: Rate of Heat Release SSE: Sum Squared of errors R²: Coefficient of determination SOI: Start of injection

SOC: Start of combustion

Figure 6: Model parameter training process

7

5

1

2

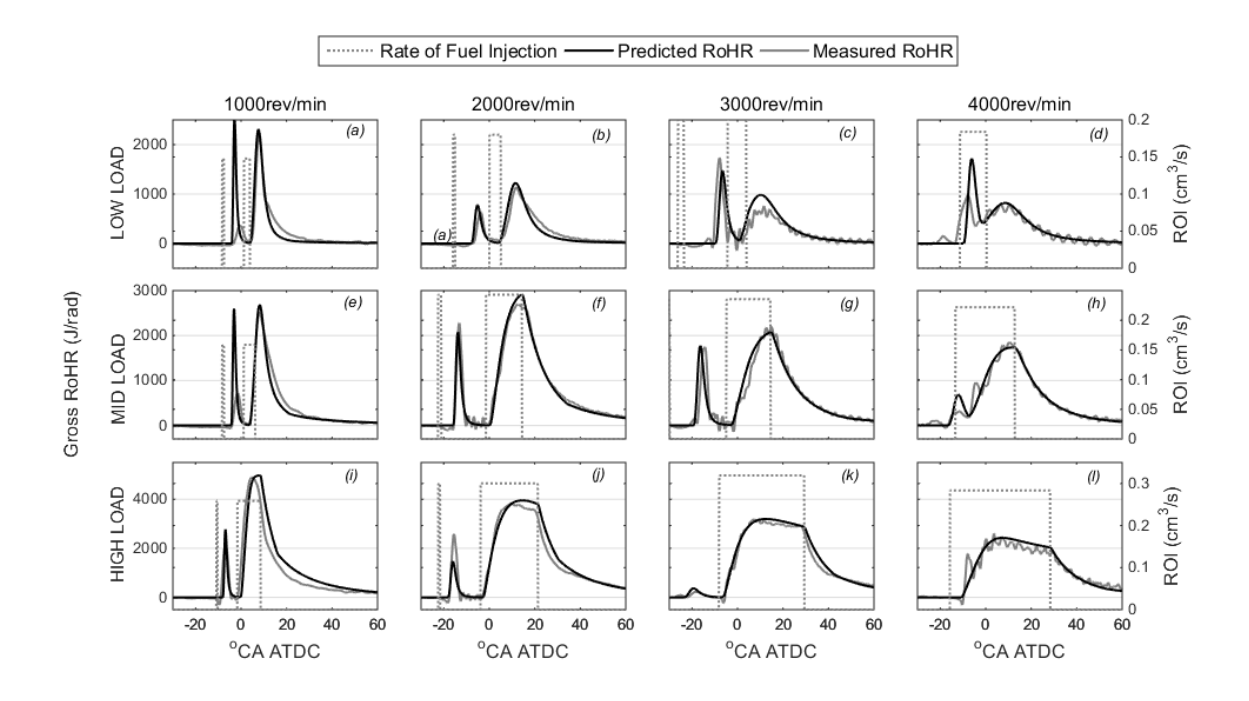


Figure 7: Rate of injection and predicted and measured gross heat release rate for a range of engine speeds and loads without EGR

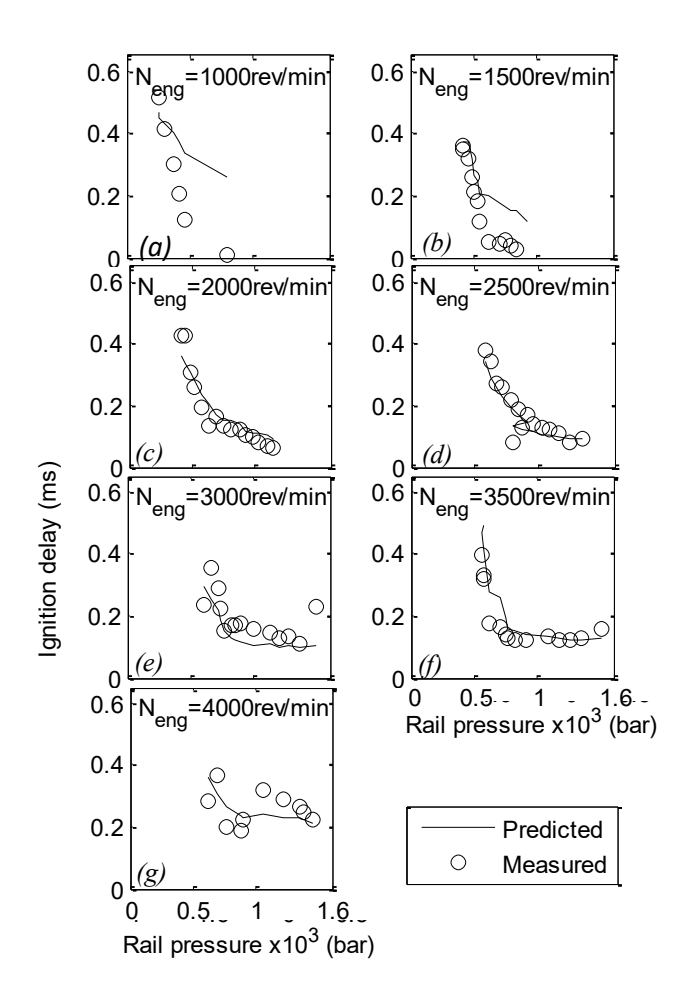


Figure 8: Measured and predicted main injection ignition delay grouped by operating speeds

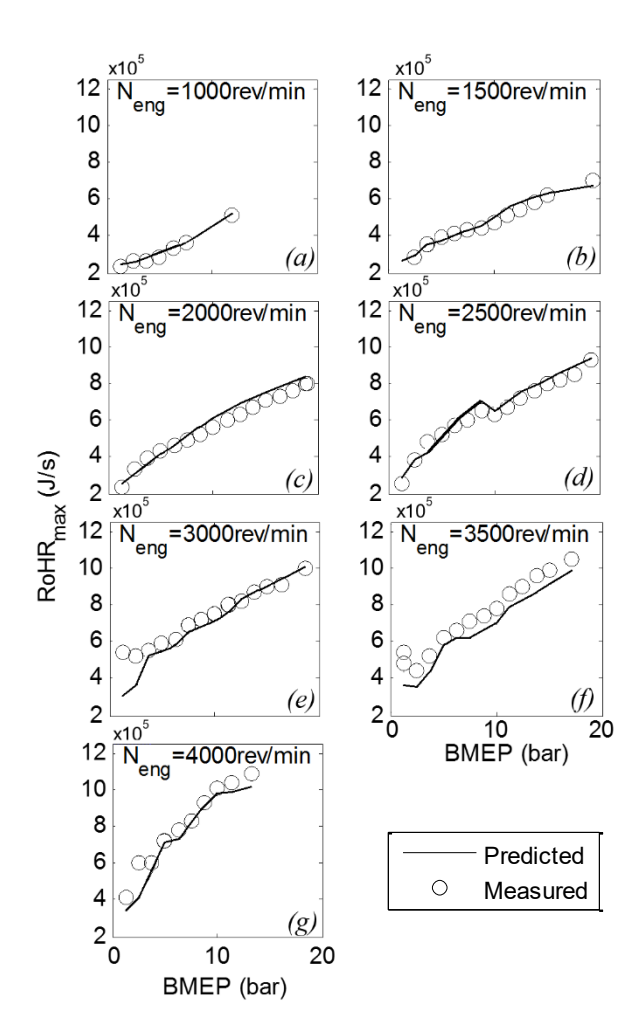


Figure 9: Measured and predicted peak heat release rate grouped by operating speeds

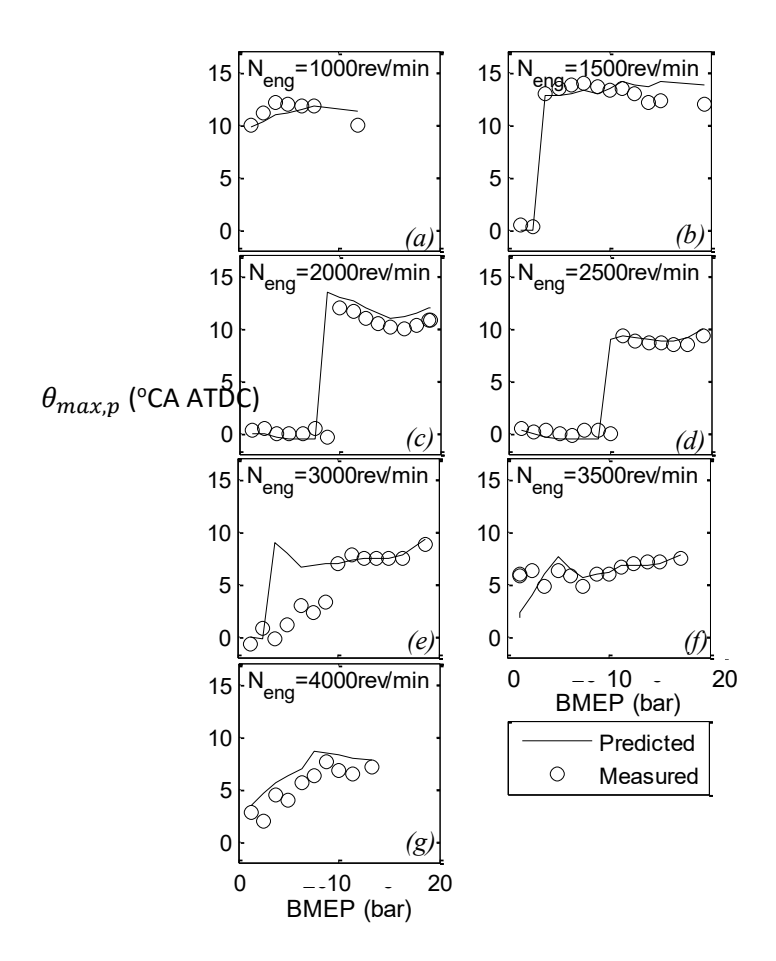


Figure 10: Measured and predicted angle of peak cylinder pressure grouped by operating speeds

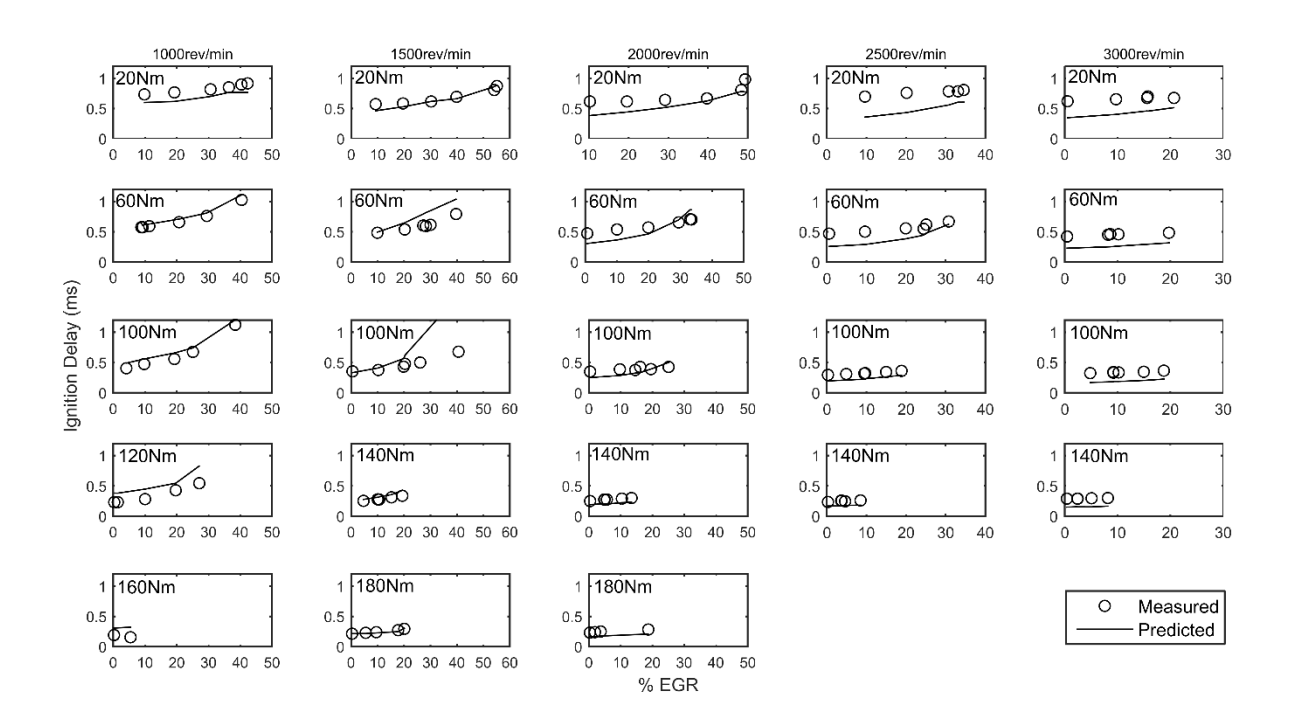


Figure 11: Measured and predicted main injection ignition delay grouped by operating speeds and load for varying EGR rates

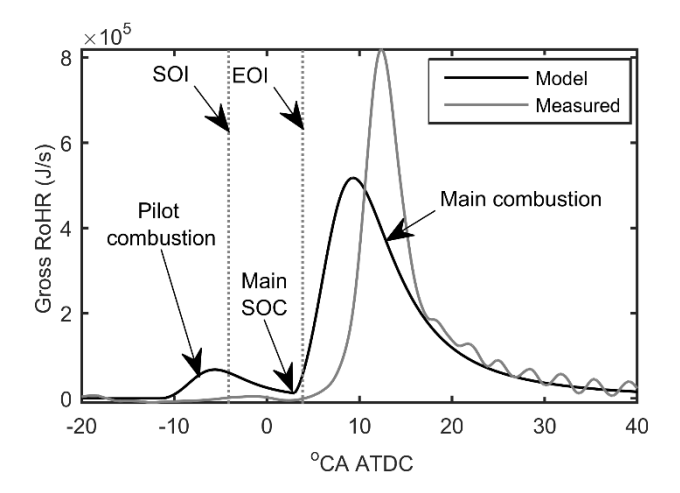


Figure 12: Example of pilot over-prediction and subsequent under-prediction of ignition delay and peak heat release rate (Engine Speed: 3000rev/min, Engine Load: 20Nm, EGR rate: 10%)

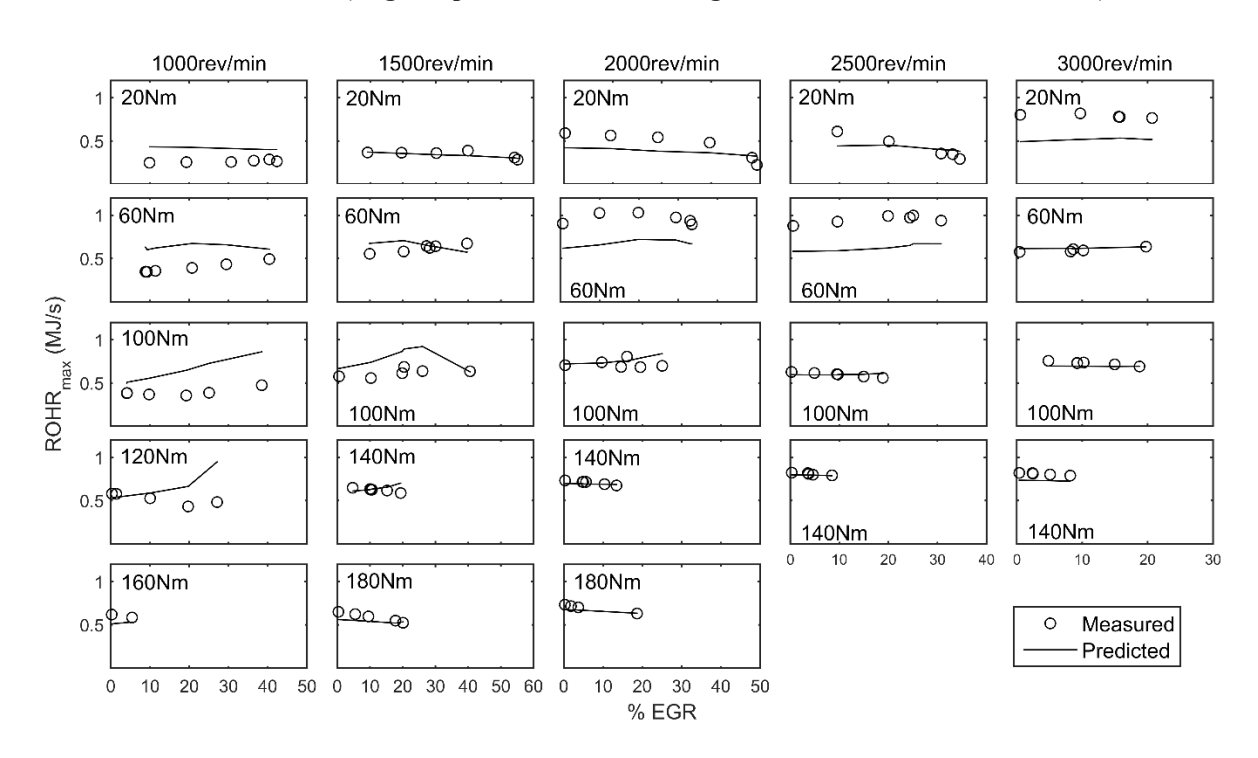


Figure 13: Measured and predicted peak heat release rate grouped by operating speeds and load for varying EGR rates

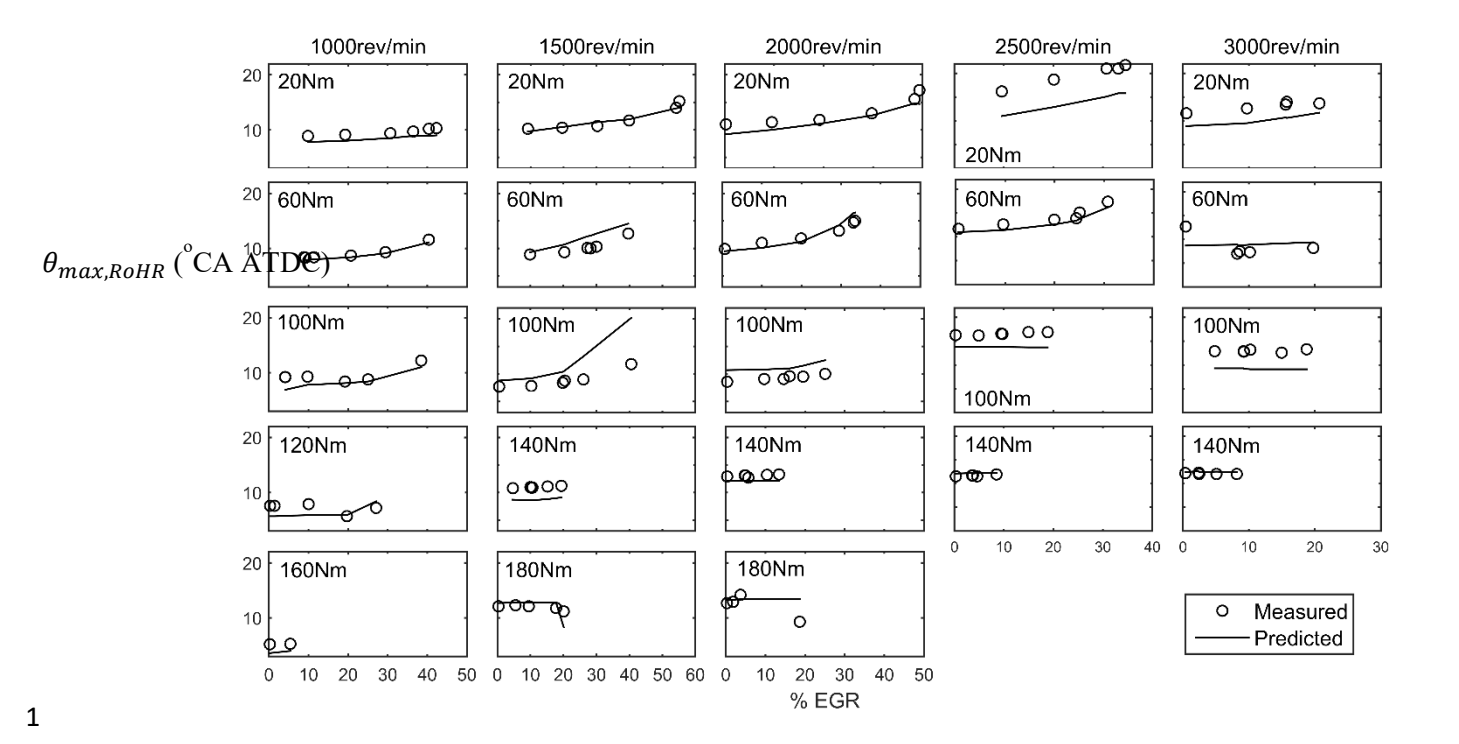


Figure 14: Measured and predicted angle of peak heat release rate grouped by operating speeds and load for varying EGR rates

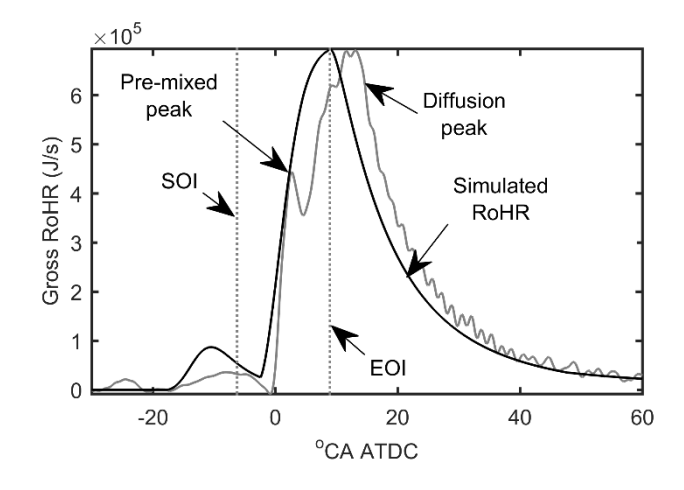


Figure 15: Illustration of the diffusion model over-prediction due to ignoring transport time between the injector nozzle and flame front (Engine Speed: 3000rev/min, Engine Load: 100Nm, EGR rate: 20%)